V European Conference on Computational Fluid Dynamics
ECCOMAS CFD 2010
M. De Gennaro, D. Caridi and M. Pourkashanian
Lisbon, Portugal, 14–17 June 2010

FFOWCS WILLIAMS-HAWKINGS ACOUSTIC ANALOGY FOR SIMULATION OF NASA SR2 PROPELLER NOISE IN TRANSONIC CRUISE CONDITION

Michele De Gennaro[*], Domenico Caridi[†], and Prof. Mohamed Pourkashanian [††]

[*]Austrian Institute of Technology, Mobility Department, Giefinggasse 2, 1210 Wien, Österreich
Ph.D. student at University of Naples Federico II, P.le Tecchio 80, 80120, Napoli, Italy
michele.degennaro.fl@ait.ac.at

[†]ANSYS UK Ltd.
6 Europa View, Sheffield, S91XH, United Kingdom
domenico.caridi@ansys.com

[††]University of Leeds, School of Process, Environmental and Materials Engineering
Woodhouse Lane, LS29JT, Leeds, United Kingdom
M.Pourkashanian@leeds.ac.uk

Key words: CFD, Aeroacoustic, Ffowcs Williams-Hawkings Acoustic Analogy, Transonic Cruise Propeller, NASA SR2.

Abstract. *Acoustic comfort is a big issue for the turboprop aircraft manufacturing industry, and therefore the development of quick and efficient numerical tools is a key point for the design-to-noise approach to airframe components. CFD approaches such as LES and DES are becoming more commonly employed in predicting aerodynamic generated noise for complex geometries, but these numerical methods are still very demanding of CPU usage for the industrial design process as used in the case of high speed propeller for turboprop applications. The goal of this paper is the simulation of propeller noise in transonic conditions based on a RANS approach for the aerodynamic computation of blade loads, coupled with Ffowcs Williams-Hawkings (FW-H) Acoustic Analogy, based on the Farassat & Brentner formulation of moving surfaces for the prediction of Sound Pressure Levels. The propeller geometry used for the calculations is the 8-blade NASA SR2 transonic propeller, chosen for the wide wind tunnel experimental data provided by NASA for different rotational speed and asymptotic Mach numbers. Results of the simulations are compared with experiments, showing the ability of this approach to predict noise with a discrepancy within a few dB for the different simulated conditions and microphones locations. Particular attention is given to the set of corrections to be applied to acoustic experimental data in order to be consistently compared with free field CFD results. The CFD simulation strategy has been refined to perform complete aerodynamics and aeroacoustic calculations with highly competitive computational cost.*

1 INTRODUCTION

In the last 20 years, the flight services market has significantly increased its business volume led by the increase of demand for fast and cheap connections among European countries. The proliferation of regional jet aircraft (e.g. A319/320/321, or B737) is a product of this trend; they are designed and optimized according to market requirements, with a passenger capacity approximately between 150 and 210 seats, and ranges between 800 and 1500 km, able to cover the most of the flight market in Europe.

Looking at the last 10 years in particular, this demand moved also towards shorter routes affected by geographical barriers (i.e. sea or mountain chains) where other solutions (i.e. trains, ferries) are not able to provide the quick and cheap service demanded.

Design trends are motivated also by the general interest from all aerospace manufacturer companies in the reduction of fuel-related costs and the environmental footprint of aircraft.

These two phenomena underlie a recent re-emergence of interest in the regional turboprop aircraft, smaller than the regional jet and able to be competitive for shorter ranges, less fuel-demanding and more environmentally respectful.

A key point in the modern turboprop industry is the comfort perceived by passenger (especially in terms of vibrations and noise), together with the increase of cruise speed of aircraft.

Looking at the recent success of the Bombardier Dash Q400, a new concept turboprop aircraft which is currently used by a number of companies in Europe, it is clear that it covers a key market window, providing a cruise speed of 670 km/h, high level of comfort experienced by passenger, together with a reduction of about 30% in fuel demand and CO_2 emissions relative to an equivalent small size turbofan aircraft [14]. Therefore we can anticipate a growing interest among all aircraft manufacturer towards the advanced turboprop concept in the coming decades, in order to increase the cruise speed up to actual turbofan standard, and improve comfort issues.

In this paper we propose a simulation methodology for propeller noise in transonic conditions based on a RANS aerodynamic approach for the simulation of the steady-state load on the blades and acoustic sources. Aerodynamic simulations were performed with the Multiple Reference Frame (MRF) approach, Pressure-Based Coupled Solver and k-ω SST turbulence model. Aeroacoustic calculations were performed with the Ffowcs Williams-Hawkings (FW-H) Acoustic Analogy, based on Farassat & Brentner's formulation of moving surfaces.

Optimized numerical settings and strategy, including periodic rotational boundary conditions and Full MultiGrid initialization (FMG), have also been an object of our investigation, in order to perform accurate aerodynamic and aeroacoustic calculations with CPU time requirements compatible with the industrial design process.

The mesh required for such simulations must be able to provide optimal y^+, an adequate number of points in the boundary layer and reliability for all experimental conditions simulated.

The propeller geometry used for the calculations is the NASA SR2 straight blade transonic cruise propeller [1,2] tested by NASA in the Lewis 8-by-6 foot transonic wind tunnel for different microphones locations and for Mach numbers from 0.6 to 0.8 and rotational speed from 6500 to 8600 rpm [3].

Calculations have been performed with the commercial software ANSYS FLUENT.

2 GEOMETRY AND EXPERIMENTAL DATA SET

Experimental acoustic data published in [3] have been used as a reference for aerodynamic and aeroacoustic simulations. The propeller blade geometry is the 8-Blades NASA SR2, a straight blade propeller constructed from the NACA 65 2D aerofoil section from root to 37% of its span extension, and from the NACA 16 2D aerofoil section from 44% to tip. The mid region is, from 37% to 44% of span, is made by a transition zone where the airfoils do not lie in any standard family.

The propeller diameter is 0.622 m (24.5 inches) and geometrical details are given in Figure 1 where Blade-Width Ratio (b/D), Ideal Lift Coefficient (C_{LD}), Design Angle ($\Delta\beta$) and Blade-Thickness Ratio (t/b) are given are given as function of blade fractional radius (r/R).

Geometrical data are provided from 24% to 100% of span and the blade root is assumed to be mounted on a cylindrical shaped body while the blade tip is assumed to be smooth. The blade angle is given by the reference design angle (measured at ¾ of span) added or subtracted to the $\Delta\beta$ curve of Figure 1.

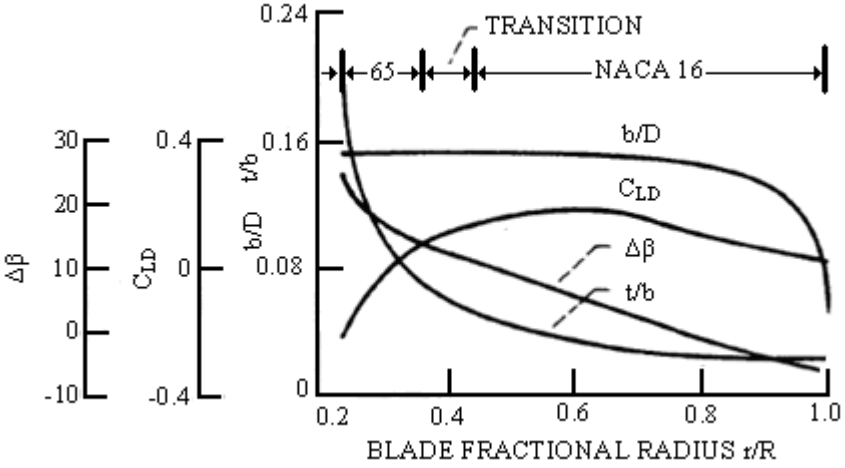

Figure 1: Geometry of NASA SR2 Propeller.

The SR2 propeller was tested in NASA Lewis 8-by-6 foot wind tunnel with a $\beta_{3/4}$ of 59 deg and mounted on an adjustable-pitch axisymmetric body used as a spinner, mounted on the tunnel ceiling with a rear support, Figure 2. The propeller was operated at nominal advance ratio J ranging from 2.75 to 3.85 for tunnel Mach numbers from 0.6 to 0.8 [3].

Nominal advance ratio J is given in (1)

$$J = \frac{V}{nD} \tag{1}$$

where V is the asymptotic velocity in m/sec, n the rotational speed in rps and D the diameter in m.

A plate was firmly attached to the tunnel ceiling at a distance of 0.3 diameters from the propeller tip, and 12 microphones were located on this plate along the longitudinal direction from a visual angle θ = 46.8 deg to 130.4 deg, where θ is the angle from propeller axis of rotation taken from the horizontal axis in front of the propeller. A

sketch of the propeller and acoustic plate device is given in Figure 2, while the microphone locations are given in Table 1 as function of Z coordinate in cm and θ in deg.

Signals from the microphones were recorded on a magnetic tape, and narrowband spectra were obtained for each point with a range from 0 to 10 KHz and a bandwidth of 32 Hz.

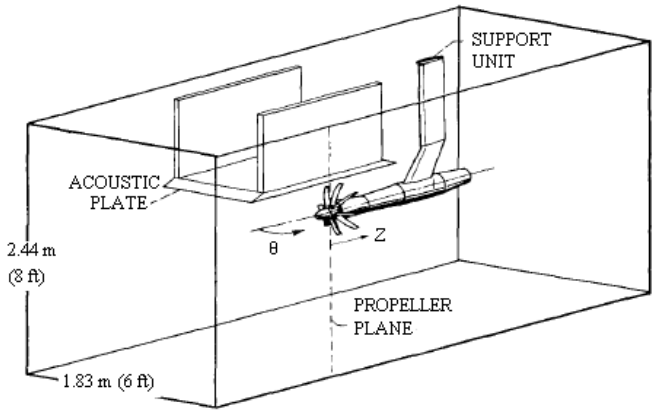

Figure 2: Sketch of NASA SR2 Propeller mounted in NASA Langley 8-by-6 foot wind tunnel.

Microphone ID											
1	2	3	4	5	6	7	8	9	10	11	12
Transducer Distance from Propeller Plane, Z [cm]											
-46.7	-41.7	-30.5	-16.0	-8.9	0.8	8.9	12.4	18.0	25.0	28.7	42.4
Visual Angle θ, from upstream (0 in front) [deg]											
46.8	50.0	58.5	72.2	80	90.9	100	104	110	116.8	120	130.4

Table 1: Microphone locations on acoustic plate device.

With reference to the data given in Table 1, the microphones are located on a straight line whose linear distance from propeller tip is 0.8 diameters. This is a key consideration in order to locate microphones in the CFD calculation, where the acoustic plate device is not modeled, and its interference effect is taken into account with a correction applied to computed SPL values as suggested by NASA [3].

3 NUMERICAL MODELLING

The propeller geometry was constructed from 6 aerofoil sections, of the NACA 65 series family for the lower part and 14 of the NACA 16 series family for the upper part.

Aerofoil sections were located with a constant spacing up to 90% of span, while a decreasing spacing was adopted up to 99% of span to follow the tip chord gradient. A smooth tip was then generated to cover the gap between 99% and 100% of span.

Aerofoil section points were imported into ANSYS GAMBIT, where NURBS lines and surfaces were generated, and the propeller was mounted on a shaped cylindrical body used as spinner, Figure 3.

A triangular surface mesh was generated in ANSYS GAMBIT on the blade and spinner, while a hybrid volume mesh was then built in ANSYS TGRID consisting of 40

prism layers and tetrahedral cells in the remaining computational domain. This approach gave a suitable value of y^+ on the blade surface for all rotational speeds considered, in general less than 1.

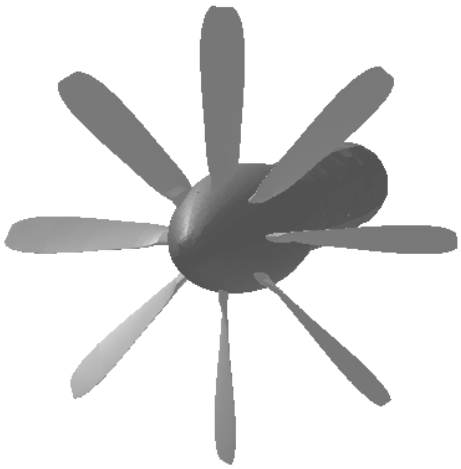

Figure 3: NASA SR2 8-blades propeller.

To reduce the total number of cells, periodic sliced domains containing only one blade were generated to simulate the isolated propeller.

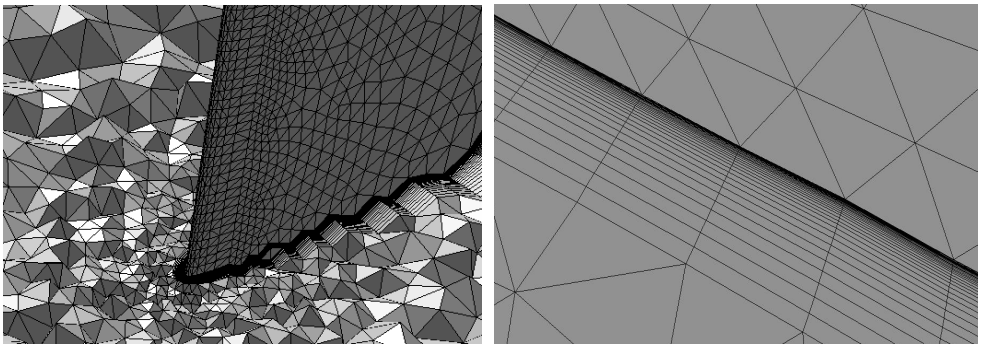

Figure 4: Grid Details

Volume mesh around the leading edge (left) – Blade suction side (right).

Prism layers were designed in order to have not less than 20 layers within the physical boundary layer, whose size was estimated by looking at the maximum reached by the Turbulent Viscosity Ratio at different stations in the span wise direction.

In fact this maximum is approximately located in the middle of the physical boundary layer, and doubling its distance from wall gives a measure of boundary layer thickness. This was done for both configurations and for all rpm conditions, generating a final mesh with the desired specifications. The final grid had 40 prism layers extruded from the blade surface mesh, with tetrahedral cells filling the rest of the fluid domain, giving a total cell count of approximately 10.5M per sliced periodic domain.

Pictures of this final grid around the leading edge and on the suction side are given in Figure 4, and an example of the Turbulent Viscosity Ratio contour used to detect boundary layer thickness is given in Figure 5.

Optimal wall y^+ value for all test conditions was also a required specification. In Figure 6, a contour of the y^+ value on the blade is given for a higher rotational speed in order to show that this value is below 1 on the whole blade surface except for a small region close to tip leading edge**.**

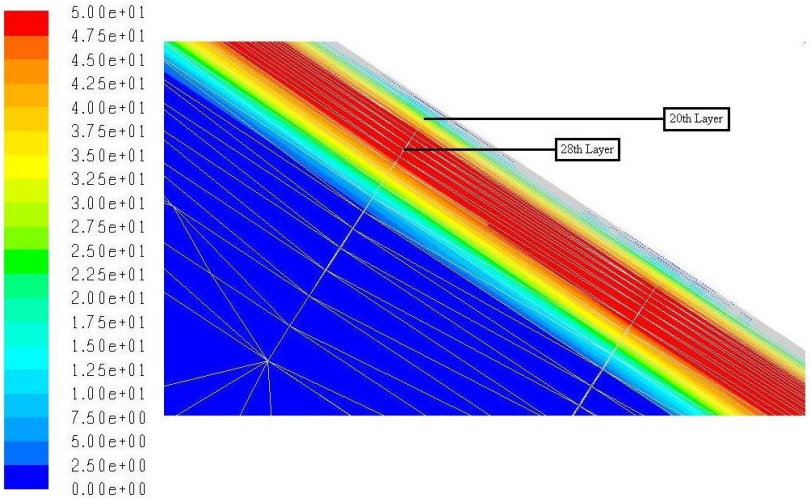

Figure 5

Turbulent Viscosity Ratio Contours, M=0.8 - 8650 RPM, 90% of Span, Pressure Side.

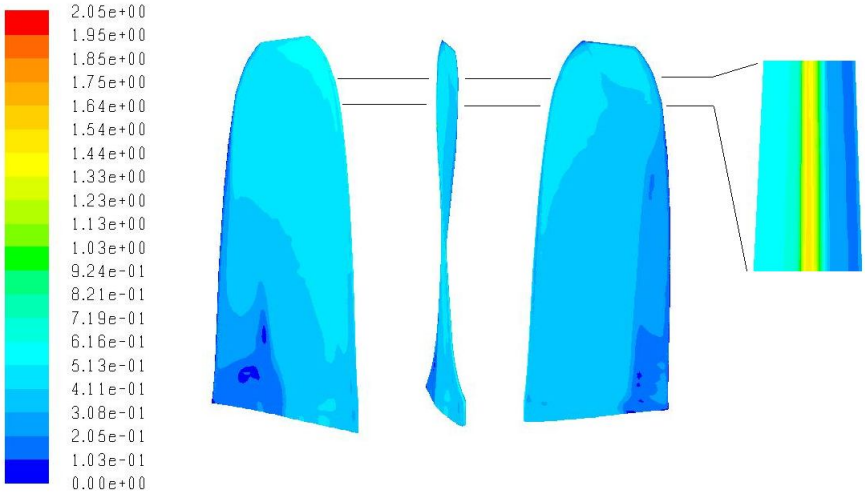

Figure 6

Y^+ contours on blade, M=0.8 - 8650 RPM.

From left to right: Suction Side, Front View, Pressure Side and Tip Leading Edge Detail (Front View).

Aerodynamic simulations were performed with the RANS Pressure Based Coupled Solver with Periodic Rotational Conditions, Multiple Reference Frame [7] and *k-ω* SST turbulence model, Table 2.

The reference blade design angle was changed in the performed simulations in order to match the experimental power coefficient C_P given by (2)

$$C_P = \frac{P}{\rho_o n^3 D^5} \tag{2}$$

where P is the power in W, ρ_o the density in Kg/m^3, n the rotational speed in rps and D the propeller diameter in m.

Fluid Model	ideal-gas
Turbulence Model	k-ω SST
P-V Coupling	COUPLED
Pressure Transport Scheme	PRESTO
Density/Momentum/k-ω/Energy	2nd order
Asymptotic Mach Number	variable
Rotational Speed	variable

Table 2: ANSYS FLUENT settings.

The acoustic Sound Pressure Level (SPL) at the microphone locations was estimated applying FW-H Acoustic Analogy, which is essentially an extension of Lighthill's equations (3) for sound pressure *p'*

$$\frac{1}{a_o^2}\frac{\partial^2 p'}{\partial t^2} - \nabla^2 p' = \frac{\partial^2 T_{i,j}}{\partial x_i \partial x_j} \tag{3}$$

to take into account noise sources related to surfaces in arbitrary motion [5,6].

The surfaces were introduced into problems multiplying the equation (3) by the Heavyside function *H(f)*, where *f=0* denotes a mathematical surface used to embed the exterior flow problem, *f>0* in an unbounded space.

The new wave equation with the surface source terms F_i and Q_i [5, 6] can be written as

$$\begin{aligned} &\frac{1}{a_o^2}\frac{\partial^2 H(f)p'}{\partial t^2} - \nabla^2[H(f)p'] = \\ &= \frac{\partial^2}{\partial x_i \partial x_j}[T_{i,j}H(f)] + \frac{\partial F_i \delta(f)}{\partial x_i} + \frac{\partial Q\delta(f)}{\partial t} \end{aligned} \tag{4}$$

and is known as the FW-H equation. It is immediately clear that if there are no surfaces (*H=1*) this reduces to equation (3).

In equation (4) the sound pressure *p'* is defined as the difference of local hydrodynamic pressure and asymptotic pressure, while a_o is the asymptotic speed of sound, δ the Dirac function, and $T_{i,j}$, F_i and Q the source terms.

The first source term $T_{i,j}$ is the Lighthill's stress tensor, related to turbulence volume noise sources, while F_i and Q are the FW-H source terms related to surface-flow

interaction noise [7]. They are given in equation (5) where $u_{i,n}$ are the fluid velocity components and $v_{i,n}$ are the surface velocity component respectively in the i-th direction and normal to surface $f=0$.

$$\begin{aligned} T_{i,j} &= \rho u_i u_j + P_{i,j} - a_o^2(\rho-\rho_o)\delta_{i,j} \\ F_i &= P_{i,j} n_j + \rho u_i (u_n - v_n) \\ Q &= \rho v_n + \rho(u_n - v_n) \end{aligned} \tag{5}$$

Finally $P_{i,j}$ is the compressive stress tensor made by static pressure plus the shear stress contribution. The surface ($f=0$) corresponds to the source (emission) surface and can be coincident with the body (impermeable) or a permeable surface, off the body surface where n_j is the normal vector pointing toward the exterior region.

Notice that in the case of an impermeable surface ($v_n=0$) and microphone fixed relative to the body ($u_n=0$), the monopole source term is dropped off.

Equation (4) is solved using the free-space Green function G (6), solution of the elementary wave propagation equation forced by time and space impulses (7).

$$G(x,t) = \frac{1}{4\pi a^2 r}\delta\left(t-\tau-\frac{r}{a}\right) \tag{6}$$

$$\frac{\partial^2 G}{\partial t^2} - a^2\nabla^2 G = \delta(t-\tau)\cdot\delta(x-y) \tag{7}$$

This solution is given in equation (8), where monopole, dipole and quadrupole source terms, respectively related to body thickness, flow interaction with moving bodies and unsteady stresses, are given. It is important to notice that monopole and dipole are related to surface integrals while quadrupoles are volume sources. This quadrupole contribution, often smaller than the other two, becomes zero for subsonic flows, and it is dropped off in the performed calculations [5].

$$\begin{aligned} &H(f)p'(x,t) = \\ &= \frac{1}{4\pi}\int_V \frac{\partial^2}{\partial y_i \partial y_j}\left[\frac{1}{|1-M_r|}T_{i,j}\left(y,t-\frac{r}{a}\right)\right]\frac{dy}{r} + \qquad \textit{Quadrupole} \\ &+ \frac{1}{4\pi}\int_\Sigma \frac{\partial}{\partial y_i}\left[\frac{1}{|1-M_r|}F_i\left(y,t-\frac{r}{a}\right)\right]\frac{dy}{r|\nabla f|} + \qquad \textit{Dipole} \\ &+ \frac{1}{4\pi a_o}\int_\Sigma \frac{\partial}{\partial t}\left[\frac{1}{|1-M_r|}Q_i\left(y,t-\frac{r}{a}\right)\right]\frac{dy}{r|\nabla f|} \qquad \textit{Monopole} \end{aligned} \tag{8}$$

One of the main advantages of the FW-H model is the possibility for it to be coupled with a steady RANS simulation for the calculation of noise sources, avoiding the need for a direct computational aeroacoustic CFD calculation. This was done using the Farassat & Brentner formulation of the FW-H acoustic analogy for moving surfaces [5, 6]. This formulation allowed us to predict an unsteady pressure time signal from a steady calculation. The time-signal transformed via FFT gave us a complete noise

spectrum but to compare simulated results and experimental data, only the maximum of SPL, coincident with the first Blade Passing Frequency (BPF), was taken into account.

This approach is of particular interest for propeller applications for the majority of operating conditions where a steady load can be assumed on the blade.

The convergence of each case was checked according to the thrust force and torque oscillation around the mean value (< 1%), obtaining a fully converged case in approximately 800/1000 iterations.

The initial simulation strategy was to simulate a gradual increase of the rotational speed, Mach number, and other settings to achieve a stable and fast convergence. For example, the following was found to give a smooth convergence:

1st Step : Segregated solver. Initialize with asymptotic flow field. Gradual increase of rpm (50→200→500→2000)
2nd Step: Gradual increase of Mach and rpm (0.1→0.4, 2000→4000, 0.4 →0.6, 4000→ 6000)
3rd Step : Switch to final Mach and rpm, switch to Pressure Based Coupled Solver

A further speed up of convergence was obtained by initializing the flow field using a Full MultiGrid technique (FMG) [7]. This consists of building up a certain number of grid levels using the Full-Approximation (FAS) Multigrid procedure [8,9]. The FMG algorithm performs an Inviscid Euler solution on the coarser grid level until a given order of residual reduction or a maximum number of cycles are reached. Then it interpolates the solution on the next finer level and solves, and so on up to the first grid level. This approach allows the time for convergence to be significantly reduced when compared to the above procedure, allowing us to skip the 1st and 2nd steps, saving up to 50% of computational cost.

4 AERODYNAMIC RESULTS

Aerodynamic simulations for transonic Mach numbers equal to 0.6 and 0.8 and cruise advance ratio of 3.06 were performed, in order to calibrate the CFD simulations against the available force experimental data. This is a common procedure in propeller aerodynamics as reported by NASA, e.g. [13].

Calibration was achieved by changing the $\beta_{3/4}$ design angle of propeller to match the experimental C_P. The experimental propeller design angle is 59 deg, and an increase of 1 deg was needed to match the experimental power coefficient for both conditions with an error in a range of some percentage points, Table 3.

Mach Number	Advance Ratio J	Rot. Speed [rpm]	$C_{P,EXP}$	$C_{P,CFD}$
0.6	3.06	6487	1.32	1.34
0.8	3.06	8650	1.51	1.57

Table 3: Comparison between Experimental and CFD Results.

An analysis of sensitivity to initial conditions and grid resolution was performed for M=0.8 only, in order to find out the dependency of the computed results on the simulation parameters. In particular the asymptotic Turbulent Viscosity Ratio and Turbulent Intensity were decreased by one order of magnitude, and mesh adaption [7] was applied between M=0.9 and M=1.1 in order to refine the cells in the shock wave region. In this sensitivity analysis, the propeller thrust and torque showed a maximum

deviation with respect to the basic case of 2% of absolute values with a percentage increase in cell number of 100% (from 10.5M to 20.1M cells).

To visualize the aerodynamic flow solution, two sections, A and B respectively, have been chosen at 30% and 90% of span extension in Figure 7. This choice was made to show the differences in flow field between the two test conditions, M=0.6 and M=0.8 respectively.

Because of the composition of the asymptotic and rotational velocity components, the propeller relative Mach number increases along the span direction. This implies that different Mach number regimes may be met by the propeller depending on the asymptotic and rotational conditions.

For the first test condition, M=0.6 and 6487 rpm, the flow field becomes locally supersonic only around the upper part of the propeller (section B) with the formation of an attached shock wave on the blade suction side (figure 8-B).

For the second test condition, M=0.8 and 8650 rpm, in the lower part of the propeller (section A) the flow field becomes locally supersonic on both pressure and suction sides, with the formation of two attached shock waves (figure 9-A). On the other hand, in the upper part of the propeller (section B) the asymptotic relative Mach number is supersonic and a detached shock wave is formed in front of the leading edge. This switch of physics around the blade happens at approximately at 60% of span extension.

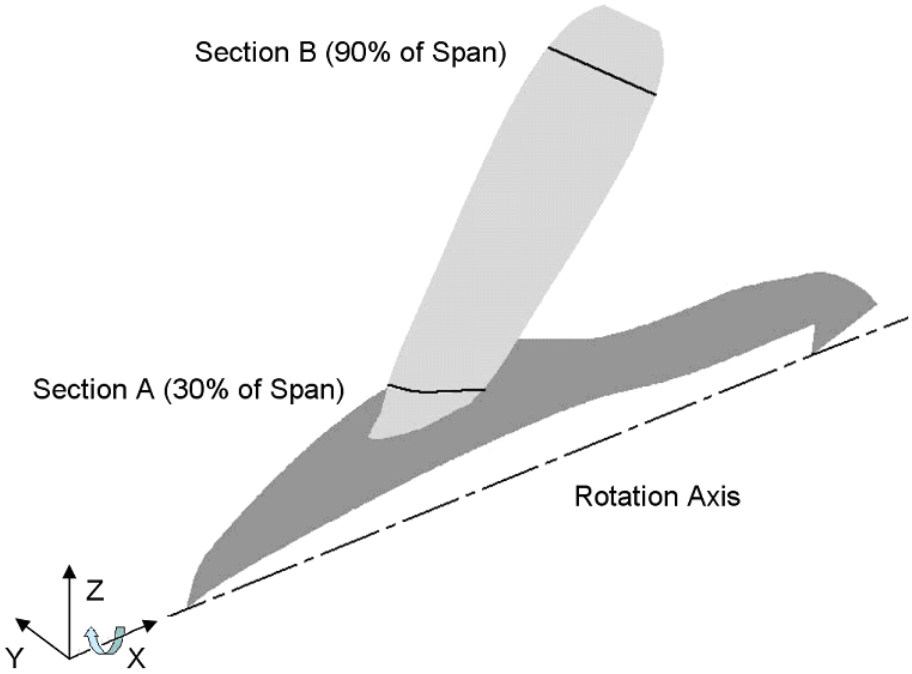

Figure 7: Section Positioning

Section A (30% of Span) – Section B (90% of Span)

The circle arrow indicates the sense of rotation.

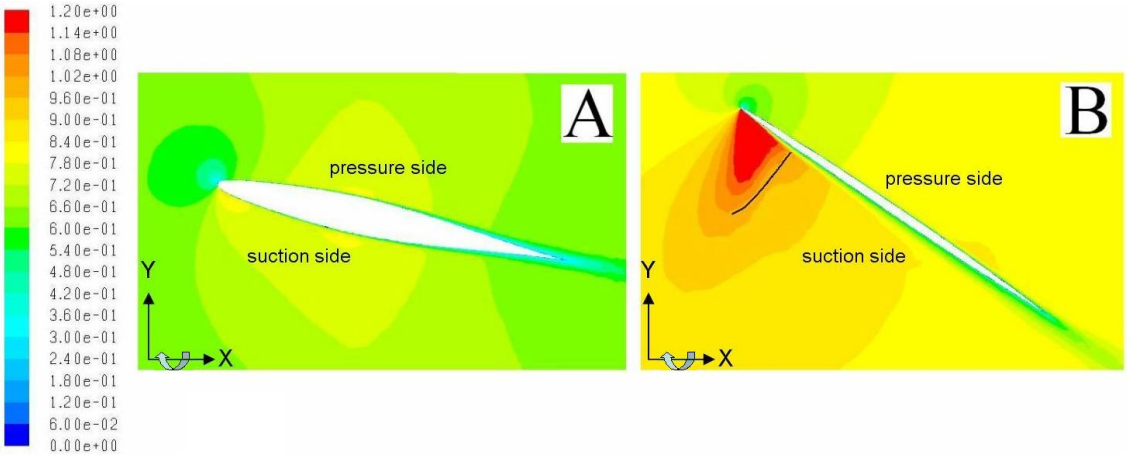

Figure 8 : Relative Mach Contours, M=0.6 - 6487 RPM

Section A (left) – Section B (right)

Black line indicates the shock wave position, circle arrow indicates the sense of rotation.

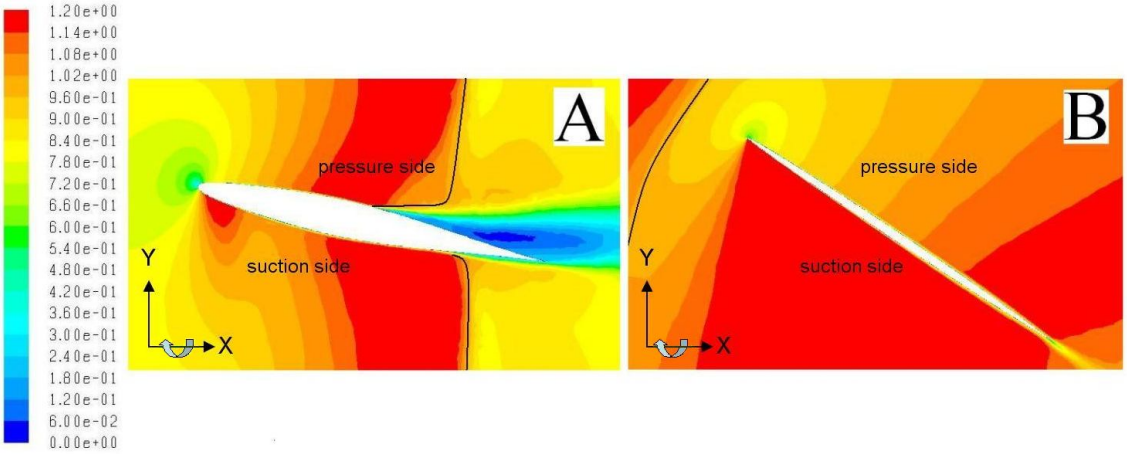

Figure 9 : Relative Mach Contours, M=0.8 - 8650 RPM

Section A (left) - Section B (right)

Black lines indicate the shock wave positions, circle arrow indicates the sense of rotation.

5 ACOUSTIC RESULTS

Noise predictions were made for the two aerodynamic conditions for 5 near-field microphones with the Farassat & Brentner FW-H acoustic analogy formulation for moving surfaces. This approach is able to give a noise spectrum from a steady RANS based simulation and the first BPF SPL was compared with experimental data available.

Simulated noise predictions were corrected to take into account some effects in the experimental data that are not simulated by our CFD computations.

In order to understand how these corrections work it is useful give a detailed discussion of how experimental data were estimated.

NASA, during the experimental campaign carried out on NASA SR propeller series, evaluated the corrections to apply to experimental data in order to scale simulations and wind tunnel tests to flight conditions [3, 4, 11]. We used these corrections to scale the CFD results to wind tunnel conditions in order to match computational and experimental data [3].

The involved corrections are:

1. Acoustic plate device interference
2. Pressure loss in wind tunnel
3. Near-Field/Far-Field SPL scaling and Pseudo-Noise
4. Wind Tunnel effects
5. Non-linear effects

These corrections played a central role in our CFD simulations in order to reduce the computational cost of our calculations as they allowed us to use the Steady RANS MRF Periodic approach coupled with FW-H acoustic analogy.

For example acoustic plate device interference and wind tunnel effects could have been simulated with Computational Aero Acoustics (CAA) modeling the noise sources and the noise propagation up to the receivers, so losing the advantages of FW-H analogy and the domain periodicity. The same could have applied for calculating the Pseudo-Noise. For capturing non-linear effects, volume quadrupole sources should have had taken into account e.g. using a permeable FW-H formulation coupled with an unsteady simulation.

According to experimental reference [3], microphones are located on an acoustic plate device, and their position is given as function of a longitudinal coordinate Z and angular coordinate θ. This positioning implies that microphones are located on a straight line at the right side of propeller, at a distance of 0.8 diameters (49.7 cm) from the blade tip.

In order to preserve the axis symmetry of the domain, we do not simulate the acoustic plate device, but we locate microphones in the same angular positions at a distance of 0.8 diameters from the propeller tip, while the acoustic plate device interference effect is taken into account with an additive SPL contribution of 8 dB [3] for all microphones.

Moreover NASA Lewis 8-by-6 foot transonic wind tunnel is affected by pressure loss depending on the test Mach number [11]. In particular, the static pressure in the test chamber is 90KPa for M=0.6 and 76KPa for M=0.8. This effect can be taken into account with the altitude correction (9) for pressure P, as provided in [4].

$$SPL_{P1} = SPL_{P2} + 20\log_{10}(P_1/P_2) \tag{9}$$

This correction is 1dB for M=0.6 and 2.5dB for M=0.8 for all microphones, according to simulations that were all performed with an asymptotic static pressure of 101KPa.

Another important correction was applied in order to extend the FW-H acoustic analogy predictions to the near-field microphones, as it is valid for far-field locations only. In this context "near field" implies the region affected by pseudo-noise.

In our case, the microphones are located quite close to the propeller, and this gives an underestimation of the computed SPL values. So the microphones were located at 16 diameters far from propeller and the SPL results were scaled to 0.8 diameters with equation (10) for correction of distance D, according to [4].

$$SPL_{NEAR} = SPL_{FAR} + 20\log_{10}(D_{FAR}/D_{NEAR}) \quad (10)$$

This correction obviously depends on how far away the microphones are located, and in the case of 16 diameters, 26 dB are needed to scale to the 0.8 diameter position. Then 1dB was added to take into account of the pseudo-noise for M=0.6 and 1.5dB for M=0.8, considering the estimates reported by NASA [4, 10].

Another correction to be taken into account is related to wind tunnel effect, estimated in 5.5 dB for M=0.6 and 2.5dB for M=0.8 according to [11].

Finally the last correction applied is related to non-linear effects for the presence of large shock waves in the flow field. One way of dealing with this is via the quadrupole source term in the acoustic analogy. The first valid analysis of the importance of the quadrupole source for high-speed rotors was made based on a two-dimensional aerodynamic calculation [12], showing how important such source effects are for the generation of additional noise in the blade section in the speed range between the critical Mach number (when flow over the aerofoil exceeds the speed of sound) and a Mach number of 1. The magnitude of this correction is in the order of a few dB as reported in reference [12] and it was estimated to be about 1dB for M=0.6 and 3dB for M=0.8 test conditions.

BPF SPL computed and corrected results are given in Figure 10 and Figure 11 for M=0.6 and 0.8 respectively. According to references [3, 4] the most accurate microphones are located approximately 20 degrees behind the propeller plane and NASA indicated these microphone locations as the least affected by repeatability errors in different test-campaigns [4, 11].

For this reason we performed calculations for microphone numbers 7 to 11, as they are considered the most accurate locations by the experimental reports.

The possibility of reducing the computational cost of RANS-FWH was investigated by performing some simulations on a coarser grid.

A new grid with only 5 prism layers and a 1.7M total cell count per sliced periodic domain was therefore generated. Simulations were performed with the MRF steady state approach, with RANS modelling and a wall function, and the Full MultiGrid Initialization technique (FMG) as used for the 10.5M cells grid. With this coarser grid a fully converged solution was obtained in approximately the same number of iterations (about 600) but with a very competitive computational time for an industrial simulation, about 5 hours on a dedicated LINUX QUAD-CORE Machine, with a 2.8GHz CPU Clock, 85% less than for the10.5M computational grid.

Simulations were performed for both Mach numbers conditions, achieving an SPL prediction within 0.5 dB of that of the 10.5M cell grid.

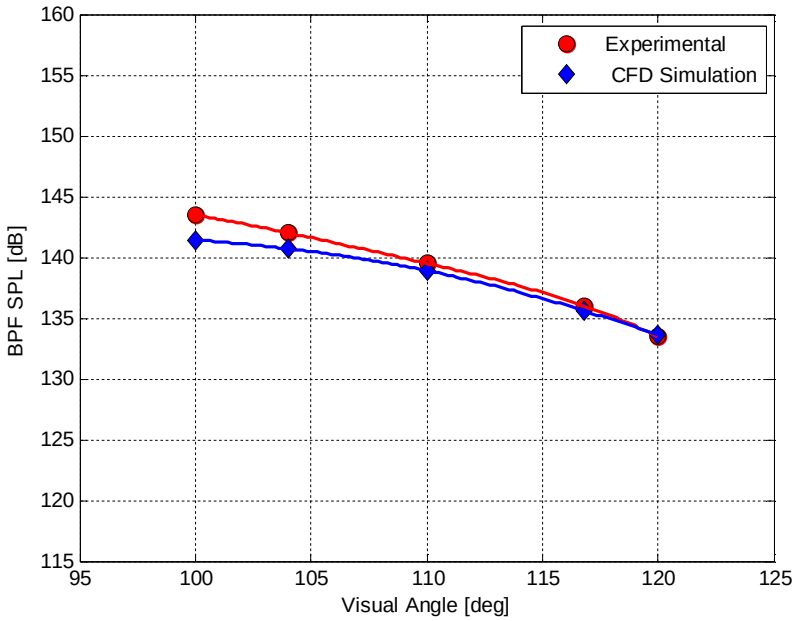

Figure 10: SPL Level of First Harmonic (BPF) -NASA SR2 (M=0.6, Rot. Speed=6487 rpm).

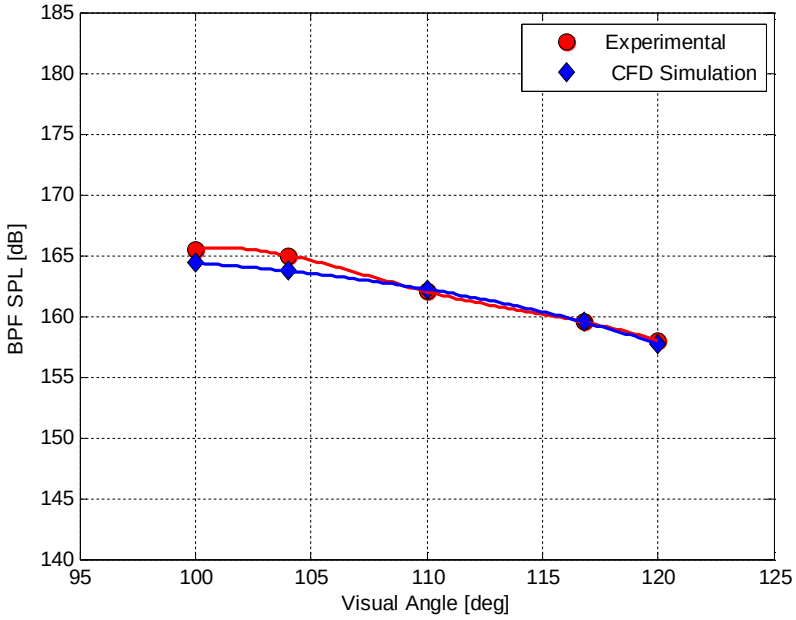

Figure 11: SPL Level of First Harmonic (BPF) –NASA SR2 (M=0.8 Rot. Speed=8650 rpm).

6 CONCLUSIONS

An extensive study was dedicated to high-speed transonic-cruise propeller noise simulation for industrial applications.

A deep exploration of the computational methods available for simulating rotors was carried out using Multiple Reference Frame, Periodic modeling approach and FMG initialization, providing a detailed description of mesh building guidelines, solver numerical settings and optimized simulation strategies.

The geometry used for this analysis was the NASA SR2 transonic cruise propeller, tested for Mach number from 0.6 to 0.8 and for rotational speed from 6500 to 8600 rpm.

A computational grid of 10.5M cells was generated with 40 prism layers on the blade to achieve optimal resolution of the boundary layer together with an optimized simulation strategy. The simulation approach adopted was RANS-MRF for the propeller aerodynamics while the FW-H acoustic analogy was used for the aeroacoustic simulation.

Acoustic Sound Pressure Levels were evaluated for 5 near-field microphones located between 10 and 30 degrees behind the propeller plane to compare computed values with wind tunnel experimental tests. In order to compare CFD results with experiments an extensive bibliographic research was necessary to determine the corrections for taking into account wind tunnel and device effects, pressure losses, near-field correction and non-linear volume sources contribution. These estimations are reported in several works from NASA.

The results show that the RANS-MRF analysis together with the FW-H Acoustic Analogy can be used to predict propeller near-field noise for NASA SR2 in transonic cruise condition providing accurate results and absolute discrepancies to experimental values of few dB (less than 2dB).

Finally RANS-MRF simulations were performed on a coarser grid of 1.7M cells, giving good results for the design condition with very fast calculation times, being able to perform a complete aerodynamic and aeroacoustic simulation in less than 5 hours on a dedicated LINUX Quad-Core machine, 2.8 GHz Core Clock.

The corrections applied may be avoidable, if the above-mentioned effects are directly taken into account, by introducing more complex simulation approaches (e.g. sliding mesh, non-periodicity, porous FW-H acoustic analogy and CAA modeling) with a significant increase in the simulation computational cost.

Future work will include the direct CFD simulation of these phenomena.

ACKOLEDGMENTS

M. De Gennaro is grateful to the EC for the support for the present work, performed within the EU FP7 Marie Curie ITN project VECOM (Grant Agreement 213543).

REFERENCES

[1] R.J. Jaracki, D.C. Mikkelson, B.J. Blaha, Wind Tunnel Performance of Four Energy Efficient Propellers, Designed for Mach 0.8 Cruise, *NASA TM-79124* (1979).

[2] G.L. Stefko, R.J. Jaracki, Wind Tunnel Results of Advanced High Speed Propellers in the Takeoff, Climb and Landing operating Regimes, *NASA TM-87054* (1985).

[3] J.H. Dittmar, Cruise Noise of the SR2 Propeller Model in a Wind Tunnel, *NASA TM-101480* (1989).

[4] C.E. Whitfield, P.R. Gliebe, R. Mani, P. Mungur, High Speed Turboprop Aeroacoustic Study (Single Rotation), *NASA CR-182257,* **Vol. 1** (1989).

[5] K. S. Brentner and F. Farassat, An Analytical Comparison of the Acoustic Analogy and Kirchoff Formulations for Moving Surfaces, *AIAA Journal 36(8),* (1998).

[6] J. E. Ffowcs-Williams and D. L. Hawkings, Sound Generation by Turbulence an Surfaces in Arbitrary Motion, *Proc. Roy. Soc. London A264 321-342*, (1969).

[7] ANSYS-FLUENT 12 User-Guide, ANSYS Inc., 2009.

[8] A. Brandt, Multi-level Adaptive Computations in Fluid Dynamics, Technical Report *AIAA-79-1455, AIAA*, Williamsburg, VA, 1979.

[9] A. Jameson, Solution of the Euler Equations for Two Dimensional Transonic Flow by a Multigrid Method, *MAE Report 1613*, Princeton University, June 1983.

[10] Sulc, J., Hofr, J., and Benda, L, Exterior Noise on the Fuselage of Light Propeller Driven *Aircraft* in Flight, *J. Sound Vib., Vol. 84, No. 1,198, pp 105-120*.

[11] J.H. Dittmar, P.L. Lasagna, H.L. Dryden, A Preliminary Comparison Between the SR-3 Propeller Noise in Flight and in a Wind Tunnel, *NASA TM-82805 (1982).*

[12] Aeroacoustics of Flight Vehicles: Theory and Practice, *NASA Reference Publication, No. 1258, Vol. 1 WRDC Technical Report 90-3052, 1991*.

[13] D.C. Mikkelson, B.J. Blaha, Design and Performance of Energy Efficient Propellers for Mach 0.8 Cruise, *NASA TMX-73612*, (1977).

[14] Bombardier Q400 website, http://www.q400.com.